Biomedical Optics EXPRESS

Quantitative analysis of intrinsic skin aging in dermal papillae by *in vivo* harmonic generation microscopy

Yi-Hua Liao,[1,2,8] Wei-Cheng Kuo,[3] Sin-Yo Chou,[3,4] Cheng-Shiun Tsai,[5] Guan-Liang Lin,[3,6] Ming-Rung Tsai,[2] Yuan-Ta Shih,[2] Gwo-Giun Lee,[5] and Chi-Kuang Sun[2,3,4,6,7,*]

[1]*Department of Dermatology, National Taiwan University Hospital and College of Medicine, National Taiwan University, Taipei 10002, Taiwan*
[2]*Molecular Imaging Center, National Taiwan University, Taipei 10617, Taiwan*
[3]*Department of Electrical Engineering, National Taiwan University, Taipei 10617, Taiwan*
[4]*Graduate Institute of Photonics and Optoelectronics, National Taiwan University, Taipei 10617, Taiwan*
[5]*Department of Electrical Engineering, National Cheng Kung University, Tainan 70101, Taiwan*
[6]*Graduate Institute of Biomedical Electronics and Bioinformatics, National Taiwan University, Taipei 10617, Taiwan*
[7]*Research Center for Applied Sciences and Institute of Physics, Academia Sinica, Taipei 11529, Taiwan*
[8]*yihualiao@ntu.edu.tw*
**sun@ntu.edu.tw*

Abstract: Chronological skin aging is associated with flattening of the dermal-epidermal junction (DEJ), but to date no quantitative analysis focusing on the aging changes in the dermal papillae (DP) has been performed. The aim of the study is to determine the architectural changes and the collagen density related to chronological aging in the dermal papilla zone (DPZ) by *in vivo* harmonic generation microscopy (HGM) with a sub-femtoliter spatial resolution. We recruited 48 Asian subjects and obtained *in vivo* images on the sun-protected volar forearm. Six parameters were defined to quantify 3D morphological changes of the DPZ, which we analyzed both manually and computationally to study their correlation with age. The depth of DPZ, the average height of isolated DP, and the 3D interdigitation index decreased with age, while DP number density, DP volume, and the collagen density in DP remained constant over time. *In vivo* high-resolution HGM technology has uncovered chronological aging-related variations in DP, and sheds light on real-time quantitative skin fragility assessment and disease diagnostics based on collagen density and morphology.

OCIS codes: (100.2000) Digital image processing; (170.0170) Medical optics and biotechnology; (170.1610) Clinical applications.

References and links

1. M. A. Farage, K. W. Miller, P. Elsner, and H. I. Maibach, "Intrinsic and extrinsic factors in skin ageing: a review," Int. J. Cosmet. Sci. **30**(2), 87–95 (2008).
2. D. Harman, "Free radical theory of aging: an update: increasing the functional life span," Ann. N. Y. Acad. Sci. **1067**(1), 10–21 (2006).
3. B. A. Gilchrest, "Age-associated changes in the skin," J. Am. Geriatr. Soc. **30**(2), 139–143 (1982).
4. R. M. Lavker, P. S. Zheng, and G. Dong, "Aged skin: a study by light, transmission electron, and scanning electron microscopy," J. Invest. Dermatol. **88**(S3), 44s–51s (1987).
5. M. Yaar and B. A. Gilchrest, "Aging of skin," in *Dermatology in General Medicine*, B. T. Fitzpatrick, I. M. Freedberg, and A. Z. Eisen eds. (McGraw-Hill, New York, 1999).
6. A. Giangreco, S. J. Goldie, V. Failla, G. Saintigny, and F. M. Watt, "Human skin aging is associated with reduced expression of the stem cell markers beta1 integrin and MCSP," J. Invest. Dermatol. **130**(2), 604–608 (2010).

#210291 - $15.00 USD Received 16 May 2014; revised 25 Jul 2014; accepted 8 Aug 2014; published 28 Aug 2014

7. K. Sauermann, S. Clemann, S. Jaspers, T. Gambichler, P. Altmeyer, K. Hoffmann, and J. Ennen, "Age related changes of human skin investigated with histometric measurements by confocal laser scanning microscopy *in vivo*," Skin Res. Technol. **8**(1), 52–56 (2002).
8. F. Timár, G. Soós, B. Szende, and A. Horváth, "Interdigitation index - a parameter for differentiating between young and older skin specimens," Skin Res. Technol. **6**(1), 17–20 (2000).
9. R. M. Lavker, "Structural alterations in exposed and unexposed aged skin," J. Invest. Dermatol. **73**(1), 59–66 (1979).
10. J. McGough-Csarny and C. A. Kopac, "Skin tears in institutionalized elderly: an epidemiological study," Ostomy Wound Manage. **44**(3A Suppl), 14S–24S (1998).
11. M. A. Farage, K. W. Miller, E. Berardesca, and H. I. Maibach, "Clinical implications of aging skin: cutaneous disorders in the elderly," Am. J. Clin. Dermatol. **10**(2), 73–86 (2009).
12. W. Montagna and K. Carlisle, "Structural changes in aging human skin," J. Invest. Dermatol. **73**(1), 47–53 (1979).
13. B. A. Gilchrest, "Age-associated changes in the skin," J. Am. Geriatr. Soc. **30**(2), 139–143 (1982).
14. J. Varani, M. K. Dame, L. Rittie, S. E. G. Fligiel, S. Kang, G. J. Fisher, and J. J. Voorhees, "Decreased collagen production in chronologically aged skin: roles of age-dependent alteration in fibroblast function and defective mechanical stimulation," Am. J. Pathol. **168**(6), 1861–1868 (2006).
15. C. E. Griffiths, A. N. Russman, G. Majmudar, R. S. Singer, T. A. Hamilton, and J. J. Voorhees, "Restoration of collagen formation in photodamaged human skin by tretinoin (retinoic acid)," N. Engl. J. Med. **329**(8), 530–535 (1993).
16. B. R. Nelson, R. D. Metz, G. Majmudar, T. A. Hamilton, M. O. Gillard, D. Railan, C. E. Griffiths, and T. M. Johnson, "A comparison of wire brush and diamond fraise superficial dermabrasion for photoaged skin. A clinical, immunohistologic, and biochemical study," J. Am. Acad. Dermatol. **34**(2 Pt 1), 235–243 (1996).
17. M. P. Goldman, N. Marchell, and R. E. Fitzpatrick, "Laser skin resurfacing of the face with a combined CO_2/Er:YAG laser," Dermatol. Surg. **26**(2), 102–104 (2000).
18. M. Gniadecka, "Effects of ageing on dermal echogenicity," Skin Res. Technol. **7**(3), 204–207 (2001).
19. M. Gniadecka and G. B. Jemec, "Quantitative evaluation of chronological ageing and photoageing *in vivo*: studies on skin echogenicity and thickness," Br. J. Dermatol. **139**(5), 815–821 (1998).
20. S. G. Lagarrigue, J. George, E. Questel, C. Lauze, N. Meyer, J. M. Lagarde, M. Simon, A. M. Schmitt, G. Serre, and C. Paul, "*In vivo* quantification of epidermis pigmentation and dermis papilla density with reflectance confocal microscopy: variations with age and skin phototype," Exp. Dermatol. **21**(4), 281–286 (2012).
21. E. M. Wurm, C. Longo, C. Curchin, H. P. Soyer, T. W. Prow, and G. Pellacani, "*In vivo* assessment of chronological ageing and photoageing in forearm skin using reflectance confocal microscopy," Br. J. Dermatol. **167**(2), 270–279 (2012).
22. C. Longo, A. Casari, F. Beretti, A. M. Cesinaro, and G. Pellacani, "Skin aging: *in vivo* microscopic assessment of epidermal and dermal changes by means of confocal microscopy," J. Am. Acad. Dermatol. **68**(3), e73–e82 (2013).
23. M. J. Koehler, K. König, P. Elsner, R. Bückle, and M. Kaatz, "*In vivo* assessment of human skin aging by multiphoton laser scanning tomography," Opt. Lett. **31**(19), 2879–2881 (2006).
24. S. Puschmann, C. D. Rahn, H. Wenck, S. Gallinat, and F. Fischer, "Approach to quantify human dermal skin aging using multiphoton laser scanning microscopy," J. Biomed. Opt. **17**(3), 036005 (2012).
25. T. Yasui, M. Yonetsu, R. Tanaka, Y. Tanaka, S. Fukushima, T. Yamashita, Y. Ogura, T. Hirao, H. Murota, and T. Araki, "*In vivo* observation of age-related structural changes of dermal collagen in human facial skin using collagen-sensitive second harmonic generation microscope equipped with 1250-nm mode-locked Cr:Forsterite laser," J. Biomed. Opt. **18**(3), 031108 (2013).
26. E. Decencière, E. Tancrède-Bohin, P. Dokládal, S. Koudoro, A. M. Pena, and T. Baldeweck, "Automatic 3D segmentation of multiphoton images: a key step for the quantification of human skin," Skin Res. Technol. **19**(2), 115–124 (2013).
27. S.-Y. Chen, S.-U. Chen, H.-Y. Wu, W.-J. Lee, Y.-H. Liao, and C.-K. Sun, "*In vivo* virtual biopsy of human skin by using noninvasive higher harmonic generation microscopy," IEEE J. Sel. Top. Quantum Electron. **16**(3), 478–492 (2010).
28. Y.-H. Liao, S.-Y. Chen, S.-Y. Chou, P.-H. Wang, M.-R. Tsai, and C.-K. Sun, "Determination of chronological aging parameters in epidermal keratinocytes by *in vivo* harmonic generation microscopy," Biomed. Opt. Express **4**(1), 77–88 (2013).
29. S.-Y. Chen, H.-Y. Wu, and C.-K. Sun, "*In vivo* harmonic generation biopsy of human skin," J. Biomed. Opt. **14**(6), 060505 (2009).
30. C.-S. Hsieh, C.-Y. Ko, S.-Y. Chen, T.-M. Liu, J.-S. Wu, C.-H. Hu, and C.-K. Sun, "*In vivo* long-term continuous observation of gene expression in zebrafish embryo nerve systems by using harmonic generation microscopy and morphant technology," J. Biomed. Opt. **13**(6), 064041 (2008).
31. N. Otsu, "A threshold selection method from gray-level histograms," IEEE Trans. Syst., Man. Cybernet. **SMC-9**(1), 62–66 (1979).
32. R. Archid, A. Patzelt, B. Lange-Asschenfeldt, S. S. Ahmad, M. Ulrich, E. Stockfleth, S. Philipp, W. Sterry, and J. Lademann, "Confocal laser-scanning microscopy of capillaries in normal and psoriatic skin," J. Biomed. Opt. **17**(10), 101511 (2012).

#210291 - $15.00 USD Received 16 May 2014; revised 25 Jul 2014; accepted 8 Aug 2014; published 28 Aug 2014

33. A. F. Frangi, W. J. Niessen, and K. L. Vincken, "Multiscale vessel enhancement filtering," Med. Image Comput. Comput. Assist. Interv. **1496**, 130–137 (1998).
34. S. Neerken, G. W. Lucassen, M. A. Bisschop, E. Lenderink, and T. A. Nuijs, "Characterization of age-related effects in human skin: A comparative study that applies confocal laser scanning microscopy and optical coherence tomography," J. Biomed. Opt. **9**(2), 274–281 (2004).
35. M. J. Koehler, S. Zimmermann, S. Springer, P. Elsner, K. König, and M. Kaatz, "Keratinocyte morphology of human skin evaluated by *in vivo* multiphoton laser tomography," Skin Res. Technol. **17**(4), 479–486 (2011).
36. S. A. M. Shuster, M. M. Black, and E. McVitie, "The influence of age and sex on skin thickness, skin collagen and density," Br. J. Dermatol. **93**(6), 639–643 (1975).
37. C. K. Sun, C. H. Yu, S. P. Tai, C. T. Kung, I. J. Wang, H. C. Yu, H. J. Huang, W. J. Lee, and Y. F. Chan, "*In vivo* and *ex vivo* imaging of intra-tissue elastic fibers using third-harmonic-generation microscopy," Opt. Express **15**(18), 11167–11177 (2007).
38. C. Boote, S. Dennis, R. H. Newton, H. Puri, and K. M. Meek, "Collagen fibrils appear more closely packed in the prepupillary cornea: optical and biomechanical implications," Invest. Ophthalmol. Vis. Sci. **44**(7), 2941–2948 (2003).
39. I. Eltoum, J. Fredenburgh, R. B. Myers, and W. E. Grizzle, "Introduction to the theory and practice of fixation of tissues," J. Histotechnol. **24**(3), 173–190 (2001).
40. M. Han, G. Giese, and J. Bille, "Second harmonic generation imaging of collagen fibrils in cornea and sclera," Opt. Express **13**(15), 5791–5797 (2005).
41. S.-W. Chu, S.-Y. Chen, T.-H. Tsai, T.-M. Liu, C.-Y. Lin, H.-J. Tsai, and C.-K. Sun, "*In vivo* developmental biology study using noninvasive multi-harmonic generation microscopy," Opt. Express **11**(23), 3093–3099 (2003).

1. Introduction

Skin aging is caused by intrinsic and extrinsic factors [1]. Intrinsic skin aging, also named chronological aging, is genetically determined and is attributable to cellular senescence or oxidative stress [2], whereas extrinsic aging is the superposition of intrinsic aging and mainly the effects of ultraviolet irradiation. Intrinsic skin aging clinically presents as atrophic skin with increased fragility and loss of elasticity [3]. Previous studies showed histologically that a consistent feature of aged skin was flattening of the dermal-epidermal junction (DEJ) with effacement of rete ridges and decrement of dermal papillary projections [4,5]. The rete ridge height decreased with age [6]. In addition, the number of dermal papillae (DP) per unit skin surface length in 90-year-old skin was reported to be less than 50% of that in 30-year-old skin [7]. The interdigitation index, a two-dimensional measurement of the interdigitation in the DEJ, was also reported to decrease with age, to an extent of about 20% between the young and elder populations [8].

The changes of dermal-epidermal interdigitation in aged skin have significant physiologic implications. The epidermis is firmly attached to the dermis at the DEJ to provide resistance against mechanical shearing forces [9]. A relatively flat DEJ results in a considerably decreased contact surface area between the epidermis and dermis, which leads to skin fragility with dermal-epidermal separation and compromises the exchange of nutrients, oxygen, and waste products between these two layers. It is in accordance with the clinical observation that aged skin is prone to be traumatized by friction and has compromised wound healing abilities [10,11].

The flattening process of the DEJ was due to the reduction of DP [12], which belongs to part of the papillary dermis. Studies have shown that intrinsic skin aging involves a number of dermal changes, including dermal atrophy, decreased collagen biogenesis, and loss of normal elastic fibers [13,14]. Although stimulation of collagen neosynthesis in the papillary dermis of photodamaged skin was observed after anti-aging treatment such as tretinoin application [15] or laser rejuvenation [16,17], no *in vivo* quantitative analysis focusing on the density of collagen fibers in the papillary dermis related to chronologically aged skin has been performed.

Although skin biopsy is the gold standard to evaluate cellular morphologic changes in dermatological studies, its invasive nature is not suitable for investigating cosmetic problems such as skin aging. Several *in vivo* instrumental devices including high frequency ultrasonography [18,19], reflectance confocal microscopy [20–22], multiphoton microscopy

#210291 - $15.00 USD Received 16 May 2014; revised 25 Jul 2014; accepted 8 Aug 2014; published 28 Aug 2014

[23,24], and second harmonic generation (SHG) microscopy [25] have been applied to assess skin aging in a noninvasive manner. Decenciere *et al.* have analyzed the morphology of the epidermis and dermis using two-photon excited fluorescence and SHG. They utilized watershed and graph cut algorithms to separate each imaging stack into three compartments: coupling medium between skin and the cover glass, the epidermis, and the dermis. Then they computed the epidermal thickness, DEJ area, collagen/elastic fiber density for young and aged groups [26]. Among these technologies, multi-harmonic generation microscopy (HGM) combining SHG and third-harmonic generation (THG) imaging modalities, has emerged as a new technique capable of assessing cutaneous morphological changes with a sub-femtoliter resolution [27]. Recently, we have successfully used *in vivo* HGM to determine chronological aging parameters in epidermal keratinocytes [28]. In the merit of the combined acquisition of SHG and THG signals of HGM, the junction between the epidermis and the dermis can be clearly observed. In addition, HGM is characterized by an adequate penetration depth up to 300 μm without photodamage, and is safe to obtain age-related alterations in the papillary dermis with a high resolution [27]. Because extrinsic skin aging is a multifactorial process influenced by environmental factors and personal habits, we primarily focused on intrinsic aging of the papillary dermis in this study. By analyzing morphological parameters of DP, we demonstrated the potential of HGM to quantify aging changes in the papillary dermis.

2. Materials and methods

2.1 Study population

Forty-eight Asians including 7 female and 8 male aged 19-29 years, 13 female and 6 male aged 30-59 years, and 8 female and 6 male aged 60-79 years, of Fitzpatrick skin phototype III or IV were enrolled. Subjects with diabetes or skin diseases were excluded. This study was conducted according to the Declaration of Helsinki Principles, and the entire protocol was approved by the Research Ethics Committee of National Taiwan University Hospital. Informed consent was obtained from each subject prior to study entry.

2.2 HGM imaging and evaluation of images

A 1230 nm femtosecond Cr:Forsterite laser was used as the excitation to minimize the attenuation in human skin and simultaneously generated second and third harmonics [29,30]. We collected backward epi-SHG and epi-THG signals to form 512 × 512 pixel image at two frames per second, with a 240 × 240 (1 ×) or 120 × 120 (2 ×) μm field of view (FOV). The transverse and axial resolutions were approximately 500 nm and 2 μm [29]. The imaging site was the volar forearm, where 90 mW average illumination power was measured. The imaging system started acquisition at 5 μm below skin surface, acquiring a frame every 5 μm until reaching the reticular dermis. In manual analysis, the 1 × data from all subjects were used. In the digital analysis, only the 2 × data from 41 subjects were used, because the image stacks of seven subjects had blurry microstructural details resulting from their involuntary motions.

For each subject, five image stacks were collected on different locations. None of our subjects reported cutaneous side effects such as erythema, pigment alteration, ulceration or blister formation. Figure 1 showed a fly-through view from the stratum corneum (SC) to the reticular dermis (RD). Moving down the skin, the SC, stratum granulosum (SG), and stratum spinosum (SS) appeared in order (Figs. 1(a)-1(c)). After the stratum basale (SB) appeared in the upper layer, the cross-sections of the isolated DP, which were the independent protrusions of the papillary dermis before it connected with other DP, were observed as independent round areas (arrows in Figs. 1(e)-1(f)), which gradually became larger and connected with neighboring isolated DP in the papillary dermis (arrowheads in Figs. 1(f)-

#210291 - $15.00 USD Received 16 May 2014; revised 25 Jul 2014; accepted 8 Aug 2014; published 28 Aug 2014

1(g)). As the region of papillary dermis expanded at the expense of SB, the lower boundary of DPZ was defined at the level where SB disappeared (Figs. 1(k)-1(l)).

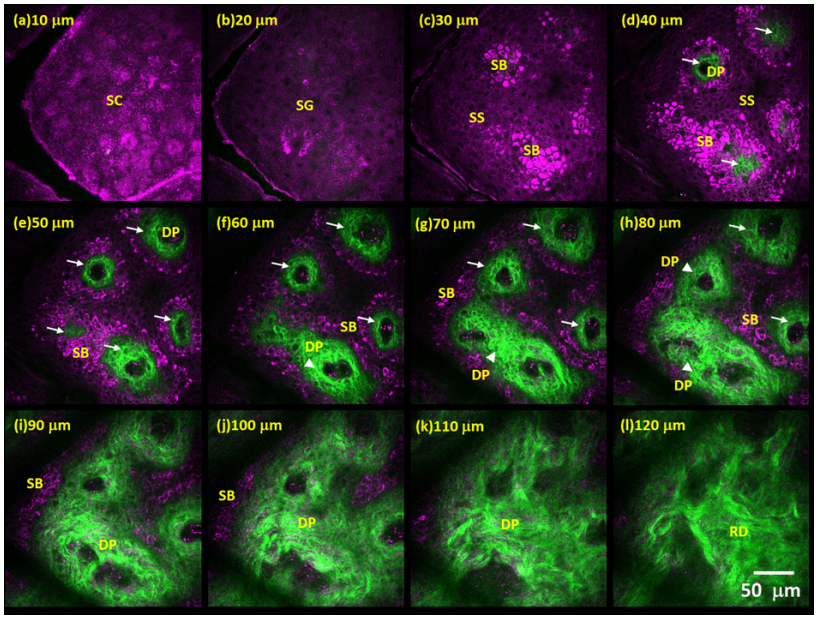

Fig. 1. A representative *in vivo* XYZ image stack obtained by HGM from the volar forearm of a 28-year-old male. (a-i) The image stack labeled at different depths included stratum corneum (SC), stratum granulosum (SG), stratum spinosum (SS), stratum basale (SB), the dermal papilla (DP) area, and the upper reticular dermis (RD). The SHG/THG signals were represented by green/purple pseudo-colors. (d-k) As the plane of observation moved down from the dermal-epidermal junction, the region of isolated dermal papilla (DP) expanded (arrows in (d)-(h)), and connected with their neighboring isolated DP in the successive frames (arrowheads in (f)-(h)). The lower boundary of DPZ was defined at the level where SB disappeared. The large circular cavities inside collagen network were the superficial capillary plexuses. (l) The reticular dermis (RD) was characterized by thick bundles of collagen fibers parallel to the skin surface. Scale bar = 50 μm.

2.3 Definition of the parameters of dermal papilla zone and manual image analysis

As shown in Fig. 2(a), we defined the green region between the two dashed lines as the DPZ, where the epidermis and dermis coexisted under HGM. The isolated DP was the independent protrusion of the papillary dermis before it merged with other isolated DP. Thus, the isolated DP represented the main part of the dermis interdigitating with the epidermis. The contact area of the dermis and epidermis was defined as the DEJ interface area. These parameters quantitatively characterized the structure of papillary dermis and had important physiologic implications. Figure 2(a) showed that the bottom dashed line presented the maximum occupied section plane of dermal papillae within the DPZ, OA_{max}, which was a normalization factor for comparing the physical properties of DPZ across image stacks. Figure 2(b) gave their formulations, where N_{total} referred to the total number of isolated DP; V_{total} was the total DP volume; C_{total} was the total collagen volume; IA_{total} was the total interface area of DEJ. N, V, and I were normalized by OA_{max} for cross-stack comparison.

In calculating the DP volume and DEJ interface area, each DP was approximated by a stack of irregularly-shaped disks. The disk thickness equaled the step size of imaging. The volume and surface area of these stacks were calculated as estimates for the DP volume and DEJ interface area, respectively. In addition, within our FOV, each complete DP contributed 1 while each incomplete DP, which was only partially visible due to limited field of view, contributed 0.5 to the total number of DP. Finally, we counted the number of frames between

#210291 - $15.00 USD Received 16 May 2014; revised 25 Jul 2014; accepted 8 Aug 2014; published 28 Aug 2014

the first observation of DP and the last observation of SB, and multiplied it with the imaging step size to estimate the depth of DPZ. We defined the 3D interdigitation index for evaluating the 3D undulation of DEJ, which was calculated by the total interface area of dermal papillae (IA_{total}) divided by OA_{max}.

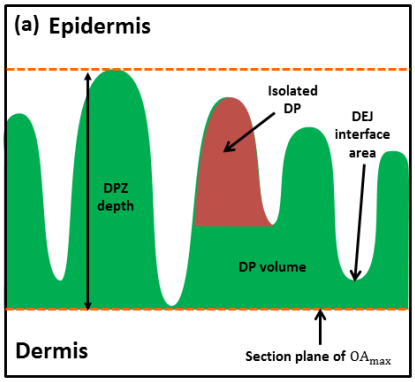

(b) Parameter	Definition
N: Number density of DP	$\frac{N_{total}}{OA_{max}}$
V: DP volume per unit area	$\frac{V_{total}}{OA_{max}}$
T: DPZ depth	The distance between the first frame of DP, and the last frame of SB
I: 3D interdigitation index	$\frac{IA_{total}}{OA_{max}}$
H: Average height of isolated DP	The average height of all isolated DP in a stack
D: Collagen density inside DP volume	$\frac{C_{total}}{V_{total}}$

Fig. 2. The parameters of dermal papilla zone (DPZ) for image analysis. (a) Definition of dermal papilla (DP) parameters in our study. (b) Formulation of these parameters. OA_{max}, the maximum occupied section area; N_{total}, the total number of DP; V_{total}, the total DP volume; C_{total}, the total collagen volume; IA_{total}, the total interface area of DEJ.

2.4 Digital image analysis for collagen density measurement

In Fig. 3, the top route represented the algorithmic framework to define the DPZ as our region of interest (ROI), and the bottom route represented the algorithmic framework to define the collagen fiber region inside ROI. The collagen density was defined as the ratio between the area of collagen fibers and that of the DPZ.

It is believed that in the papillary dermis, bright SHG signal corresponds to the collagen-rich region [27,29]. Therefore we utilized the intensity information of image to segment ROI. As collagen network was rich in holes, we first performed gray-scale dilation using a circular disk as our structural element because it was isotropic and sufficiently large to fill up the holes. Then we passed the image through a small 2D Gaussian low-pass filter to smooth the sharp edges introduced by dilation. The two steps effectively filled up collagen mesh holes without causing significant ROI expansion.

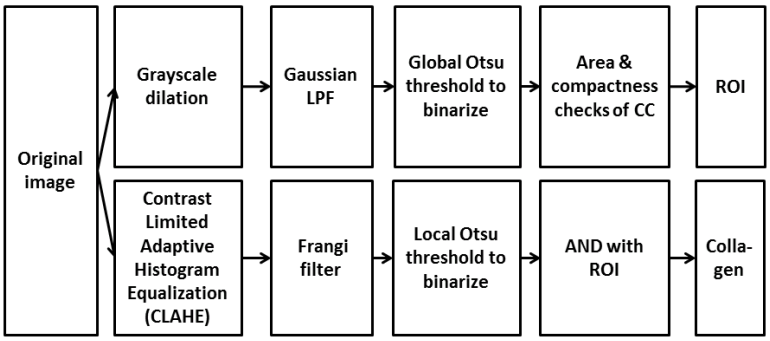

Fig. 3. Algorithmic framework. We segmented the region of DPZ as our region of interest (ROI) in the top route, and the collagen structure in the bottom route. Then we defined the 2D collagen density as the ratio of the area of collagen fibers to the ROI area. CC, connected components; LPF, low pass filter.

#210291 - $15.00 USD Received 16 May 2014; revised 25 Jul 2014; accepted 8 Aug 2014; published 28 Aug 2014

Next, since our collagen image roughly had three classes of intensity, i.e. white for dense collagen, gray for loose collagen, and black for non-collagen areas, we applied 3-class Otsu global threshold to segment the smoothed image into 3 groups [31]. We used Otsu's threshold because it is an unbiased threshold that optimizes the ratio of between-group to within-group variance. Otsu model nicely matches the intrinsic property of our data, which is composed of three categories of pixels: collagen, intensity-saturated collagen, and background noise.

We applied Otsu's threshold globally to maintain the connectivity of ROI. Despite its high sensitivity to poor-SNR collagen, local threshold would tear ROI into pieces and require substantial work to bring them back. To binarize the image, we defined the top 2 classes in 3-class Otsu-thresholded images as potential collagen areas and set them to 1. In the binary image, we evaluated each negative connected component's (CC) descriptors, including 1) area, and 2) compactness. Here are the criteria we used to include CC into ROI, where A denotes CC area, CD denotes capillary diameter, and P denotes compactness. The subscript l denotes lower bound, and u denotes upper bound:

$$A < CD_l, \tag{1}$$

$$CD_l < A < CD_u \bigcap P < P_{thr}. \tag{2}$$

Equation (1) states that CCs smaller than a particular threshold are treated as collagen network mesh holes and included in ROI. The capillary cavity referred to the disk-shape dark area in Fig. 4(d). We estimated the diameter of papillary capillaries to be 6-16 μm (31-82 pixels). It covers the entire range of known diameter 7-12 μm of skin capillary [32], so it is unlikely to include papillary capillary region in the ROI. The grayscale dilation and smoothing effectively reduced the cavity diameter by 7 pixels, meaning the capillary cavity area became 450 (CD_l) ~4400 (CD_u) pixels, where each pixel width is 0.2 μm (assuming the cavity is a circular disk). In Eq. (2), we evaluated the compactness of the CCs with areas in the range of capillary cavities. Here compactness is defined as:

$$P \equiv \frac{Perimeter^2}{A}, \tag{3}$$

where Perimeter is the number of boundary pixels that enclose the CC by 8-connectivity. For a perfect disk, the compactness value is $(2\pi r)^2/(\pi r^2) = 4\pi$. We set the compactness threshold P_{thr} as 8π to allow some deviation of cavity section shape from a perfect disk. Any negative CC within the capillary area range but with compactness smaller than 8π will be left outside ROI. Otherwise it will be treated as collagen mesh holes standing for the dermal matrix and included in ROI. For CCs with areas larger than upper capillary area bound, we treated them as the spacing between different collagen networks and removed from ROI. The entire process was shown in Fig. 4.

#210291 - $15.00 USD Received 16 May 2014; revised 25 Jul 2014; accepted 8 Aug 2014; published 28 Aug 2014

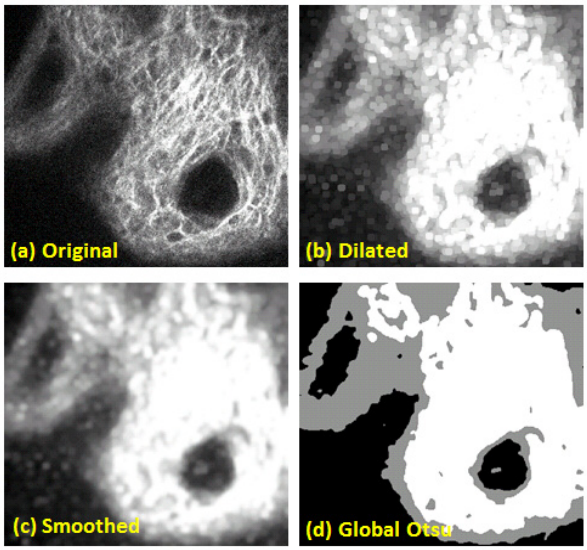

Fig. 4. ROI segmentation. (a) Original image. (b) Dilated image. (c) Smoothed dilated image. (d) Three-class global Otsu image. The top two classes, the gray and white regions, were considered as the collagen fiber areas. The capillary cavity is the big round dark region at the lower right corner of images (b-d). Note that collagen region with weak intensity was well preserved in the ROI segmentation.

The bottom route produced collagen segmentation by first applying the contrast limited adaptive histogram equalization (CLAHE), which removed the random contrast in images due to SHG mechanism and manual tuning of photon multiplier tubes. Then the Frangi filter was used to extract the cylindrical structure of collagen fibers [33]. The idea of Frangi filter is to evaluate the second order derivatives at each pixel, and to compute the eigenvalues of its Hessian matrix. The eigenvectors gave us the principal axes of the point's neighborhood structure, while the sign of eigenvalues told us whether the point is a local maximum or minimum. The notable vesselness function in [33] is,

$$v(s) = \exp(\frac{-R^2}{2B^2})(1-\exp(\frac{-S^2}{2C^2})) \quad (4)$$

where B and C are thresholds to control the sensitivity of the detected R, the ratio of larger to smaller eigenvalues, and S, the Frobenius matrix norm of eigenvalues [33]. Here R is defined as the ratio of Hessian matrix eigenvalues, always above one. The Frangi filter has been proven to be a powerful tool in detecting cylindrical structure. In practice, we used minimal Frangi filter scales on collagen image to make the Frangi-filtered fiber as delicate as the one in original image.

As the original image was intrinsically 3-class, we also observed that the Frangi filtered image was also 3-class. This inspired us to apply 3-class Otsu's threshold to Frangi filtered images. Simple global thresholding was not sufficient for fiber extraction because we had inhomogeneous intensities throughout the image, which made purely intensity-based segmentation schemes error-prone. As means to cope with inhomogeneous intensity, we not only applied CLAHE and Frangi filter, but broke the image into 4 × 4 tiles before we applied the Otsu threshold. We used local threshold here instead of global threshold because Frangi-filtered fiber had strong structureness, and would not be torn in pieces due to local thresholding. When binarizing Otsu image, we chose the white and gray region as our collagen fiber similar to ROI segmentation process, and set them to 1. Next, we performed logic AND on the binary image and its corresponding ROI to set out-of-ROI pixel to 0,

#210291 - $15.00 USD Received 16 May 2014; revised 25 Jul 2014; accepted 8 Aug 2014; published 28 Aug 2014

because we were interested in the collagen within ROI only. The process was shown in Fig. 5. Finally, we summed up the collagen area and ROI area respectively in every frame and stack and computed the ratio of collagen area to ROI area as collagen density.

To demonstrate the importance of unbiased Otsu threshold schemes, we performed a *P*-value test by replacing the 3-class Otsu threshold in our density analysis algorithm by $\text{Mean} \pm X * \text{Std}$ of image, where Std stands for standard deviation, and X is the variable. The third Otsu class corresponds to pixels with intensity value in $[\text{Mean} + X * \text{Std}, \infty]$; the second Otsu class, $[\text{Mean} + X * \text{Std}, \text{Mean} - X * \text{Std}]$; the first Otsu class, $[\text{Mean} - X * \text{Std}, -\infty]$. The plot of the age-dependent density analysis *P*-value against X is shown in Fig. 6. Another thresholding schemes based on order statistics, e.g. thresholds at (25th, 75th) percentile of image intensity, have similar threshold-dependency as shown above.

From Fig. 6, we concluded that the *P* value of collagen density analysis was highly sensitive to the choice of thresholds. This implies that to use hand-tuned intensity threshold runs the risk of not just erroneous collagen segmentation, but also highly threshold-dependent statistical results.

2.5. Statistical analysis

The result of the DP parameters was expressed as mean ± standard deviation. The value of correlation coefficient between age and DP parameters was calculated using a Pearson linear regression model. One-way analysis of variance (ANOVA) was used for comparisons among three age groups. Statistics were performed with the SPSS12.0 software (SPSS Inc., Chicago, IL), and $P < 0.05$ was considered statistically significant.

3. Results

3.1 In vivo image analysis of age-dependent alterations in the dermal papilla zone

Figures 7(a)-7(d) showed the correlation between age and parameters N, T, V, I. Each data point represented a subject in the form of mean ± SD (standard deviation) computed from all the stacks. One-way ANOVA test compared three age groups, 19-29, 30-59, and 60-79 years old (Figs. 7(e)-7(h)). For the number density of DP, the *P* value calculated by the linear regression analysis was 0.950, showing no statistically significant correlation with age (Fig. 7(a)). The number density of DP for the three age groups were 149.88 ± 55.07 mm^{-2}, 149.54 ± 49.58 mm^{-2} and 146.14 ± 55.85 mm^{-2}, respectively, without statistically significant difference (Fig. 7(e); $P = 0.81$, one-way ANOVA). In contrast, a negative correlation was found between the depth of DPZ and age (Fig. 7(b); **, $P < 0.01$, $r = -0.46$). The depths of DPZ for three age groups were 74.22 ± 13.25 μm, 60.63 ± 16.32 μm, and 57.20 ± 14.29 μm, respectively, showing that aging flattened DEJ (Fig. 7(f); **, $P < 0.01$, one-way ANOVA). Unexpectedly, the volume of DP per unit area was not correlated with age (Fig. 7(c); $P = 0.15$). Parameter V for age groups 19-29, 30-59, and 60-79 were 39.09 ± 8.12 μm, 34.55 ± 10.76 μm, and 34.55 ± 12.04 μm, respectively, without statistically significant difference (Fig. 7(g); $P = 0.40$, one-way ANOVA). Negative correlation existed between the 3D interdigitation index and age (Fig. 7(d); **, $P < 0.01$, $r = -0.58$). The index for the three age groups were 2.734 ± 0.378, 2.389 ± 0.554, and 2.089 ± 0.291, respectively. The interface area of DEJ decreased with age (Fig. 7(h); **, $P < 0.01$, one-way ANOVA), reflecting smoother undulation of DEJ in older skin.

#210291 - $15.00 USD Received 16 May 2014; revised 25 Jul 2014; accepted 8 Aug 2014; published 28 Aug 2014

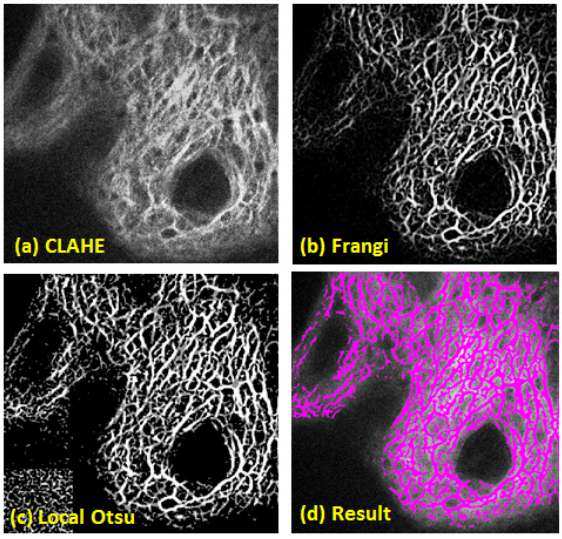

Fig. 5. Collagen segmentation. (a) Original image enhanced by CLAHE. (b) Frangi-filtered image. (c) 3-class local Otsu image in 4x4 tiles. (d) Collagen segmentation overlaid on original image. The cylindrical structure of collagen was well-preserved.

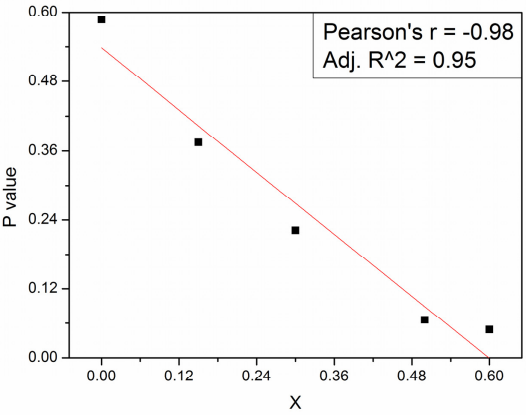

Fig. 6. Plot of *P*-value against tunable threshold parameter X. Note the strong correlation between threshold parameter and *P*-value, suggesting that hand-tuned thresholds are not suitable for SHG collagen statistical study.

Figure 8 showed a negative correlation between the average height of isolated DP and age (Fig. 8(a); **, $P < 0.01$, r = –0.49). The average height of isolated DP for age groups 19-29, 30-59, and 60-79 were 21.90 ± 5.98 μm, 15.01 ± 4.85 μm, and 14.25 ± 4.11 μm, respectively, supporting the conclusion of regression analysis (Fig. 8(b); **, $P < 0.01$, one-way ANOVA). In addition, we performed one-way ANOVA for all parameters and found statistically significant gender difference in the average height of isolated DP only, the mean of which was 18.91 μm in male and 15.54 μm in female subjects ($P < 0.05$). Figures 8(c)-8(e) showed 3D visualization of the isolated DP height and the flattening of it over time. The depth of DPZ and the 3D interdigitation index decreased with age as well. The results of representative 3D reconstruction were consistent with Figs. 7(c), 7(d), 7(g), 7(h) and Figs. 8(a)-8(b).

#210291 - $15.00 USD Received 16 May 2014; revised 25 Jul 2014; accepted 8 Aug 2014; published 28 Aug 2014

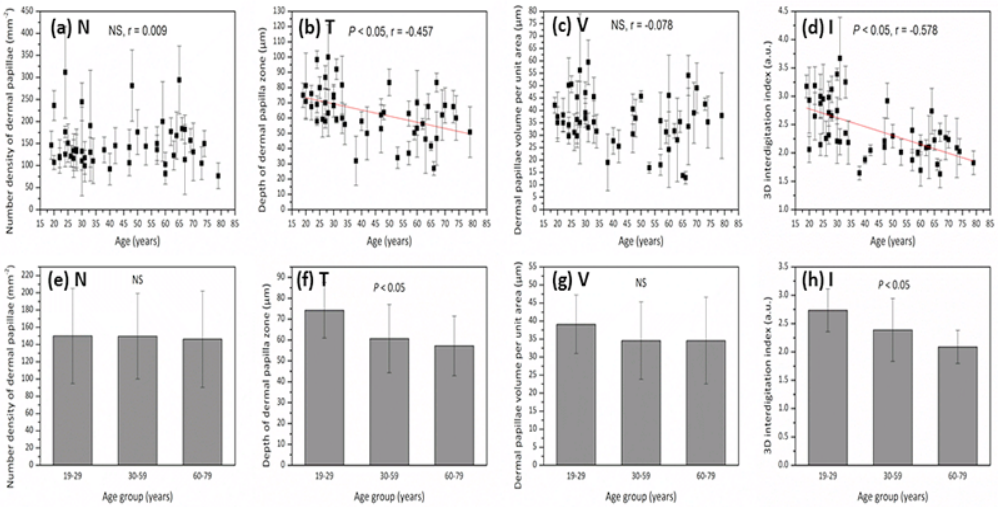

Fig. 7. The depth of dermal papilla zone and the 3D interdigitation index were negatively correlated with age. The results of linear regression (a, c, e, g) and ANOVA analysis (b, d, f, h) for number density of dermal papillae (N), depth of dermal papilla zone (T), DP volume per unit area (V), and the 3D interdigitation index (I). (a, b) No significant correlation was found between N and age. (c, d) T significantly decreased with age. (e, f) V showed no correlation with age. (g, h) Parameter I was negatively correlated with age. NS, not significant. **, $P < 0.01$. The data were presented as mean ± standard deviation.

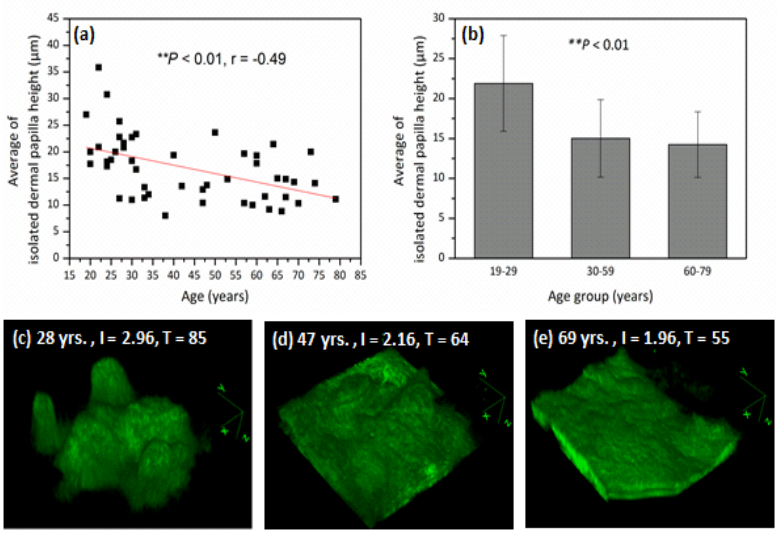

Fig. 8. The average height of isolated dermal papilla significantly decreased with age. (a) Linear regression analysis; **, $P < 0.01$. (b) ANOVA analysis in three age groups; **, $P < 0.01$. Representative 3D reconstructions of the dermal papilla zone (DPZ) obtained from the volar forearm of (c) 28-, (d) 47-, (e) 69-year-old subjects. Only SHG signals from XYZ image stacks within the DPZ were used in the reconstruction, which revealed the structure of isolated dermal papillae. The coordinate axes were added beside the reconstructions with the z-axis pointed to the lower dermis. It was shown that the average height of isolated dermal papilla (H), the depth of DPZ (T), and the 3D interdigitation index (I) decreased with age.

3.2 Digital image analysis for collagen density in the dermal papilla zone

Figure 9 showed the output image and density values of collagen density algorithms, which effectively identified cylindrical collagen structures. The data of Figs. 9(a) and 9(c) came

#210291 - $15.00 USD Received 16 May 2014; revised 25 Jul 2014; accepted 8 Aug 2014; published 28 Aug 2014

from a 20-year-old male and a 63-year-old male, respectively. Our experiment showed that the collagen density in DPZ did not change with age. The collagen densities for three age groups were 0.355 ± 0.020, 0.353 ± 0.039, and 0.373 ± 0.031, respectively. The *P* values of linear regression and one-way ANOVA for collagen density were 0.072 and 0.308, respectively, showing no statistically significant correlation or difference with age (Figs. 9(e) and 9(f)). We summarized the key findings of our study in Table 1.

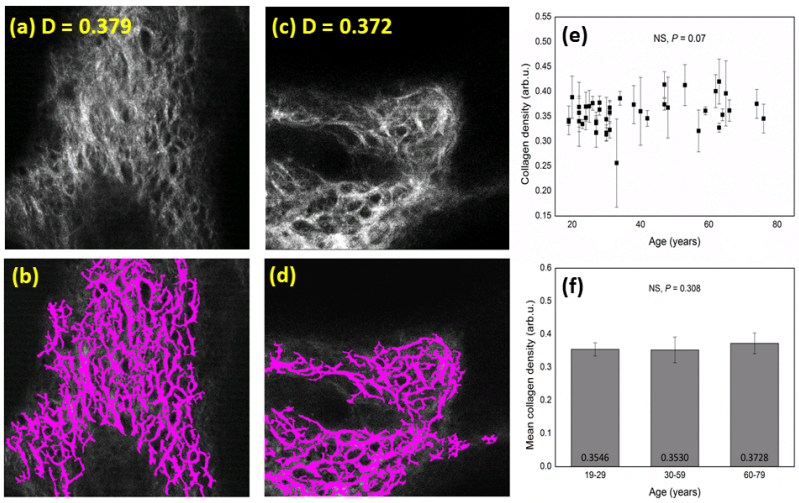

Fig. 9. The collagen density of the dermal papilla zone over volar forearms was not significantly altered with age. (a, c) The CLAHE-enhanced images. (b, d) The results of binary collagen segmentation overlaid on original images. The match between collagen segmentation and the original image is great. (a, b) The collagen density in a 20-year-old male was calculated to be 0.379, meaning that collagen occupies 37.9% of the DPZ. (c, d) The collagen density in a 63-year-old male was calculated to be 0.372. The density values matched our intuition that subfigures a and c had similar collagen density. (e, f) Statistical analyses of the outputs of density analysis algorithm with age by linear regression (e) and one-way ANOVA (f). No significant correlation could be found. The data were presented as mean ± standard deviation.

Table 1. Correlation between age and DPZ parameters

Parameters	N	V	T	I	H	D
Correlation	Not significant	Not significant	Negative correlation	Negative correlation	Negative correlation	Not significant

4. Discussion and conclusion

With unprecedented spatial and temporal resolution *in vivo*, our study could potentially serve as a benchmark to compare with previous DP studies. A previous study indicated that the depth of DPZ decreased with age on Caucasians by confocal microscopy [34], consistent with our study on Asians. In addition, the 2D interdigitation index was shown to decrease with age based on skin biopsy sections [8], which was consistent with our result of the 3D interdigitation index. However, we did not observe the decrease in the number of DP with age in volar forearm as reported by many studies based on *in vivo* confocal microscopy or multiphoton microscopy [7, 20, 35]. The difference might arise from the skin phototype of the subjects [20], which we limited to only type III and IV, the DP calculation method, and the characteristics of HGM. For HGM, a sharp contrast between SHG and THG signals, adequate penetration, and high resolution could increase the sensitivity to detect the flattened DP in older skin.

Compared with Decenciere's work [26], our study is novel in several aspects. First, we proposed the protocol for manually analyzing the morphology of papillary dermis and

#210291 - $15.00 USD Received 16 May 2014; revised 25 Jul 2014; accepted 8 Aug 2014; published 28 Aug 2014

characterized it with new parameters, e.g. the height of isolated DP, the volume of DP per unit area, and the density of collagen fibers in the DPZ. In addition, due to the exact and refined measurement achieved by *in vivo* HGM, the standard values or ranges of these dermal papilla parameters in different age groups have been set up. These quantitative results will help in understanding the mechanics of dermal-epidermal interactions as well as its consequence of compromised skin during aging processes. Second, we defined the collagen density in 2D image, and provide an image segmentation scheme for collagen fibers and the surrounding network region. The use of Otsu threshold obviates ad hoc threshold tuning that affects density. In addition, the Frangi filter we used leverages second-derivative structure of image topography to provide a robust collagen density measure across a substantial range of image contrast and noise levels. Third, our clinical study was performed on 48 subjects evenly aged from 18 to 79. The statistical analysis based on linear regression and one-way ANOVA yielded reliable *P* values and provided critical physiologic and therapeutic implications in dermatological fields as follows.

First of all, very different from the 2D impression derived from the traditional histology of the skin, we first demonstrated that the DP density, the DP volume per unit, and the collagen density in the DPZ were not decreased but simultaneously remained unchanged during processes of intrinsic aging using an *in vivo* 3D HGM measurement. If previous studies were correct that dermal collagen density decreased over time [36], the loss could mainly occur in the reticular dermis or resulted from photoaging instead [25]. Our findings that no significant collagen volume loss occurred in the papillary dermis over time also indicated that replenishing collagen in the papillary dermis by cosmetics or instrumental procedures may not be useful to resume the aging changes of DP. Second, chronological skin aging caused the decrease in the 3D interdigitation index, the average height of isolated DP, and the depth of DPZ, while kept the DP volume, number density of DP, and collagen density in the DPZ unchanged. We thus propose that in the process of intrinsic aging, instead of total disappearance of DP, the originally tall DP become flattened to form shorter and wider DP without alteration in volume nor number density. Nevertheless, the contact surface between the epidermis and dermis is significantly decreased with advancing age, which results in impairment of mechanical resistance and nutrient deficiency in the epidermis, and can contribute to the formation of skin ulcerations and interfere with wound healing processes. The cause of intrinsic aging-associated DP flattening is unknown but may result from shrinkage and sagging of the terminal elastic fiber arcades which distribute in the papillary dermis and extend to the epidermis in young people as demonstrated by electron microscopy [12]. The quantitative HGM measurement of elastic fibers [37] related to aging requires further studies.

In addition to SHG microscopy, other imaging methods for dermal collagen analysis include X-ray diffraction, histology, and electron microscopy [38–40]. Each has its limitations. First, X-ray diffraction is invasive and fails to visualize collagen network [38]. Histology and electron microscopy both require invasive biopsy, fixation, and staining processes. Despite being time-consuming, fixation tends to change the tertiary structure of collagen proteins [39]. SHG microscopy comes to overcome the drawbacks of these methods, because collagen is a non-centrosymmetric triple helix highly capable of SHG [40]. Similar to multiphoton microscopy, SHG occurs in tightly focused volume and yields high spatial resolution to achieve 3D imaging without slicing and labeling. However, different from the multiphoton fluorescence process, higher harmonic generation processes excited with a ~1230 nm pulsed Cr:forsterite laser are virtual-transition-based, and therefore no photodamage and photobleaching effects are observed [41]. With high safety profiles, high resolution and a superior signal-to-noise ratio at depths, HGM is suitable for *in vivo* dermal collagen imaging.

#210291 - $15.00 USD Received 16 May 2014; revised 25 Jul 2014; accepted 8 Aug 2014; published 28 Aug 2014

Acknowledgments

The project is funded by National Health Research Institute of Taiwan under NHRI-EX102-9936EI and National Taiwan University under 102R891601.

#210291 - $15.00 USD Received 16 May 2014; revised 25 Jul 2014; accepted 8 Aug 2014; published 28 Aug 2014